

# Synthesis and characterization of polypyrrole/vanadium pentoxide nanocomposite aerogels

H. P. Wong,<sup>a</sup> B. C. Dave,<sup>b</sup> F. Leroux,<sup>c</sup> J. Harreld,<sup>a</sup> B. Dunn<sup>\*a</sup> and L. F. Nazar<sup>c</sup>

<sup>a</sup>Department of Materials Science and Engineering, University of California, Los Angeles, Los Angeles, CA 90095-1595, USA

<sup>b</sup>Department of Chemistry and Biochemistry, Southern University of Illinois at Carbondale, Carbondale, Illinois, USA

<sup>c</sup>Department of Chemistry, University of Waterloo, Canada, Waterloo, Ontario, Canada N2L 3G1

Vanadium pentoxide/polypyrrole aerogel (ARG) composites have been synthesized by sol-gel routes, and investigated as cathode materials in Li batteries. The primary method utilized simultaneous polymerisation of pyrrole and vanadium alkoxide precursors. Hydrolysis of VO(OC<sub>3</sub>H<sub>7</sub>)<sub>3</sub> using pyrrole-water-acetone mixtures yielded monolithic green-black gels with polypyrrole/V ratios ranging from 0.15 to 1.0. Supercritical drying yielded high surface (150–257 m<sup>2</sup> g<sup>-1</sup>) aerogels with densities between 0.1 and 0.2 g cm<sup>-3</sup>, that were of sufficient mechanical integrity to allow them to be cut without fracturing. TEM studies of the ARGs show that they are comprised of fibers similar to that of V<sub>2</sub>O<sub>5</sub> ARGs, but with a significantly shorter chain length. The interaction between the polypyrrole (PPy) and V<sub>2</sub>O<sub>5</sub> aerogel in the nanocomposites was probed using IR spectroscopy. Our results suggest that the inorganic and organic components strongly interact during the initial stages, thus perhaps impeding the vanadium condensation process. Hence, the PPy/V<sub>2</sub>O<sub>5</sub> nanocomposites exhibited lower electrical conductivity with increased polypyrrole content. The addition of (NH<sub>4</sub>)<sub>2</sub>S<sub>2</sub>O<sub>8</sub> as an oxidizing agent improved the conductivity of the nanocomposites. The deleterious effect of the conductive polymer on the bulk conductivity does not necessarily affect the electrochemical properties of these materials. Nanocomposite materials that were subjected to post-oxidative treatment show enhanced Li insertion capacity compared to the pristine ARG. The physical properties of these 'nanocomposite aerogels' are different from 'microcomposites' prepared by an alternate route, in which the oxide gel is formed in the presence of a dispersion of preformed micrometer-sized polypyrrole particles.

Supercritical drying of monolithic V<sub>2</sub>O<sub>5</sub> gels formed from the rapid hydrolysis of vanadium alkoxides yields aerogels (ARGs) that display extremely high surface areas and controllable porosity.<sup>1</sup> These characteristics make them attractive as cathodes in rechargeable lithium batteries where kinetic barriers due to Li access and transport within the crystalline lattice can pose limits to attaining theoretical capacities.<sup>2</sup> Their low electrical conductivity can be minimized by the use of extremely thin films supported on a conductive substrate, or partially overcome by the incorporation of conductive carbon additives. Li batteries comprising electrodes of these materials demonstrate relatively high lithium insertion capacity and energy density.<sup>3</sup> Nevertheless, neither of these methods fully capitalize on the high surface area available in the materials. A potential alternative to the addition of carbon is the incorporation of a conducting polymer into the ARG structure. Polypyrrole (PPy) is an electronically conductive polymer which has received considerable attention due to its high electrical conductivity and stability in electrochemical environments. PPy also has been shown to be a promising cathode in lithium secondary cells,<sup>4</sup> although maintenance of surface area and hence access of ions to the polymer structure remains a difficulty in this pseudo-capacitive type material.<sup>5</sup> The support of PPy on high surface area V<sub>2</sub>O<sub>5</sub> aerogels thus offers the prospect of maximizing the performance of both inorganic and organic components.

Fabrication of these materials in monolithic form presents some challenges. The synthesis of low surface area xerogel V<sub>2</sub>O<sub>5</sub>-polymer nanocomposite crystallites is well established. Amongst the most interesting materials are those of polyaniline<sup>6</sup> and polypyrrole<sup>7</sup> in which the polymer chains have been interleaved between the V<sub>2</sub>O<sub>5</sub> sheets by an *in situ* intercalation and oxidative polymerisation method. At high polymer content, these materials show improved conductivity compared to pristine V<sub>2</sub>O<sub>5</sub> xerogels. Our recent electrochemical studies on

these nanocomposites,<sup>8</sup> in addition to similar studies of polyaniline nanocomposites of HTaWO<sub>6</sub><sup>9</sup> and MoO<sub>3</sub>, have all shown enhancement in lithium ion mobility on incorporation of the polymer.<sup>10</sup> These findings have prompted us to develop methods for the synthesis of ARG-based polymer/oxide composites.

Our strategy described here involves *in situ* polymerisation of the pyrrole monomer during the sol-gel condensation process. A preliminary account of this work has been reported.<sup>11</sup> The oxidative coupling of the pyrrole units (by the vanadium oxide) to form PPy, is simultaneous with polymerisation of the inorganic oxide which is catalysed by reaction with the pyrrole. The result is a monolithic inorganic-organic hybrid gel in which both components are mixed at the nanocomposite level. For comparison, we have also investigated *in situ* encapsulation of preformed colloidal particles of PPy within the V<sub>2</sub>O<sub>5</sub> gel, during the initial stages of the sol-gel condensation process. This method yields a monolithic homogeneous 'micro'composite of the V<sub>2</sub>O<sub>5</sub> and PPy. Our investigation probes the interaction of the inorganic and organic components of these ARGs, its effect on the electrical properties, and on electrochemical Li insertion into the nanocomposite ARG.

## Experimental

### Synthesis and physical properties

Vanadium pentoxide ARGs containing polypyrrole were synthesized using two variations of the sol-gel method. Both methods are based on our prior work involving the hydrolysis and condensation of vanadium isopropoxide (Gelest) in acetone-water solutions.<sup>1</sup> In the first method (simultaneous polymerisation), the alkoxide and pyrrole (Aldrich) were mixed,

and a vial containing the mixture was placed in an ice bath along with a vial containing the water–acetone mixture. A typical composition was 1.0 VO(OC<sub>3</sub>H<sub>7</sub>)<sub>3</sub>:40 H<sub>2</sub>O:17 (CH<sub>3</sub>)<sub>2</sub>CO:yC<sub>4</sub>H<sub>4</sub>NH. The two vials were allowed to cool prior to mixing, after which the water–acetone mixture was stirred into the vial containing the alkoxide and pyrrole. Samples without pyrrole were also prepared. The sol was stirred and cast into rod-shaped glass vials. Gelation occurred within 75 s without pyrrole to yield transparent dark red gels; the pyrrole containing materials gelled within 10–30 s resulting in deep green opaque gels. The ratio of pyrrole (P) was varied from 0.15 to 1.0 mol VO(OR)<sub>3</sub>, and the water–acetone molar ratio was also varied extensively over a wide composition range to obtain compositions PPy<sub>2P</sub>V<sub>2</sub>O<sub>5</sub>. This resulted in ARGs with sufficient mechanical integrity to allow the monolithic samples to be cut into discs with a diamond saw for measurements of bulk electrical conductivity. Some preparations also involved the pre-oxidation of the pyrrole monomer with (NH<sub>4</sub>)<sub>2</sub>S<sub>2</sub>O<sub>8</sub> (0.075 mol l<sup>-1</sup>) prior to its reaction with the alkoxide.

V<sub>2</sub>O<sub>5</sub>/polypyrrole microcomposite ARGs were synthesized by forming the oxide gel in the presence of a dispersion of the preformed PPy. This approach is in contrast to others reported in which pyrrole is polymerized *in situ* around dispersed particles of oxide<sup>12</sup> or carbon black.<sup>13</sup> Pyrrole was polymerized in a 2.5 M solution of iron(III) chloride in diethyl ether (FeCl<sub>3</sub>:Py, 4:1 mol) according to the procedure used by Myers.<sup>14</sup> The precipitated PPy was vacuum dried for 4 h at 65 °C and ground into a fine powder. The conductivity of the polymer thus prepared was 54 S cm<sup>-1</sup>, as determined by two-point ac conductivity measurements on pressed pellets (see below). The desired quantity of polymer was then added to a solution of water and acetone. A relatively stable dispersion was formed by mixing the solution using an automatic stirrer at 8000 rpm. Vanadyl triisopropoxide and the polymer dispersion were chilled to 0 °C in separate containers. The polymer dispersion was poured into the casting vial containing the vanadyl alkoxide (V:H<sub>2</sub>O:acetone, 1:40:18 mol), shaken quickly and allowed to gel. Gelation occurred within 10 s. The resulting composite gels were treated as described above.

The wet gels were aged for 4 days in their sealed containers with a 1 mm hole in the cap, to allow for slow evaporation of the solvent within the wet gel. This resulted in a small amount of shrinkage (15%) and densification that strengthened the gels. After aging, the gels were removed, and immersed in acetone for a day to promote exchange of the water in the gel pores for acetone. This procedure was repeated four times to ensure complete exchange. The gels were transferred to the pressure vessel (Polaron E3000 Critical Point Dryer) for supercritical extraction by CO<sub>2</sub>.<sup>1</sup> The resultant dark-green cylinder-shaped monoliths had dimensions of *ca.* 1 cm in diameter, and 3 cm in length.

The density of the aerogels was determined using a pycnometer vial filled with Hg. Surface area measurements (N<sub>2</sub> absorption) were conducted on a Micromeritics Flowsorb 2300 system and analyzed by the BET method. The nanocomposite powders were vacuum dried at 125 °C for 3 h prior to degassing the samples. TGA (Dupont 9900 Thermal Analysis System) measurements were used to determine molar composition of the pyrrole/V<sub>2</sub>O<sub>5</sub> gels. Analysis of the materials was performed in N<sub>2</sub> and air using a heating rate of 10 °C min<sup>-1</sup> to 600 °C. TEM was performed on a Phillips CM30. Samples were prepared by dipping holey carbon grids into a sonicated dispersion of the ARG fragments in hexane. FTIR data were obtained as KBr pellets on a Nicolet FTIR spectrometer operating between 400 and 4000 cm<sup>-1</sup>. Samples of V<sub>2</sub>O<sub>5</sub> and PPy<sub>2P</sub>V<sub>2</sub>O<sub>5</sub> ARGs were prepared for detailed FTIR spectroscopy, using <sup>18</sup>O-labeled water and deuterium-labeled water (D<sub>2</sub>O). X-Ray powder diffraction (XRD) patterns of the crushed ARGs were obtained on a Siemens D500 X-ray

diffractometer equipped with a diffracted beam monochromator, using Cu-K $\alpha$  radiation. Samples were scanned at a step scan rate of 0.02° s<sup>-1</sup>.

## Electrical and electrochemical measurements

Aerogel discs were used to measure electrical conductivity. The discs were coated with gold at both ends using a plasma sputtering system (Anatech, Ltd. Hummer VI-A). Two-point ac complex impedance measurements (20 Hz–1 MHz) were performed using a computer-controlled Hewlett Packard 4284A Precision LCR meter using a 0.1 V root mean square test signal, and ensuring ohmic contact. The discs were heated at 150 °C for 24 h prior to taking measurements. Variable temperature conductivity measurements were made in the range from 180 to 25 °C in flowing argon (99.995%).

To study Li insertion in the materials, composite electrodes were prepared from active material, carbon black (Super S, Alpha Chemicals) and Kynar Flex 2820–00 as the organic binder. The powders in the mass proportion 80, 15, 5, respectively, were mixed in cyclopentanone and the slurry was spread onto an aluminium disk. Before assembling the cells in the glove box, the composite electrodes were heated at 80 °C for 3 h in order to remove the free water without altering the morphology of the ARGs. A solution of 1.0 M LiClO<sub>4</sub> in propylene carbonate (PC, Aldrich) was used as the electrolyte. The PC was twice distilled under vacuum from activated molecular sieves through a glass-bead filled column prior to its use. Swagelok type cells were assembled in an argon filled glove box containing <2 ppm of water and oxygen. Electrodes had a surface area of 1.0 cm<sup>2</sup> and contained *ca.* 2 mg of active material.

A multichannel galvanostatic/potentiostatic system (MacPile<sup>®</sup>) was used for the electrochemical study. Voltage was applied in steps of 10 mV (0.2 h)<sup>-1</sup> and 10 mV (0.02 h)<sup>-1</sup>; alternatively, in the galvanostatic mode, the voltage dependence *vs.* Li composition for the composite electrode was studied under varying current densities. The most common corresponded to an intercalation of 1 Li in 20 h.

The electronic density (per mol V<sup>-1</sup>) *vs.* voltage was calculated by numerical differentiation of the voltage composition dependence curves. The charge cycle is denoted by positive values. For low current densities, the dx/dV *vs.* V curves give identical information to a cyclic voltammogram, in terms of position of Li potential sites and their relative occupancies.

## Results

### Synthesis

Fig. 1 is a composition map for the polypyrrole/V<sub>2</sub>O<sub>5</sub> nanocomposites with a fixed pyrrole ratio of 0.15 (corresponding to a composition PPy<sub>0.3</sub>V<sub>2</sub>O<sub>5</sub>). Water and acetone ratios were varied over a wide range which enabled us to obtain monolithic, homogeneous gels with good mechanical integrity. Optimum properties were found in the range corresponding to samples 5–9. Higher water ratios and lower acetone ratios produced more robust gels, but increased the gelation rate. Increased pyrrole concentration decreased the strength of the gels, although this could be compensated by a higher water ratio and lower acetone ratio. Improved integrity was also achieved by partially drying the wet gel during the aging treatment under ambient conditions prior to supercritical drying. This resulted in slight densification of the ARGs compared to those which were not subjected to this treatment. For pure V<sub>2</sub>O<sub>5</sub> ARGs, the partial drying treatment produces samples with densities in the range of 0.2 g cm<sup>-3</sup> as compared to 0.1 g cm<sup>-3</sup> obtained without the treatment. The addition of pyrrole has little effect on ARG density, as the [PPy]V<sub>2</sub>O<sub>5</sub> ARGs (all partially dried) exhibited slightly increased densities of *ca.* 0.2 g cm<sup>-3</sup> (Table 1).

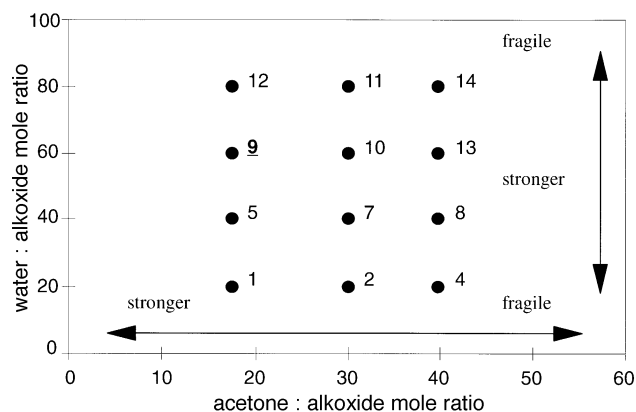


**Fig. 1** Compositions of nanocomposites synthesized with a pyrrole ratio of 0.15. The arrows represent the relative mechanical integrity of the gels.

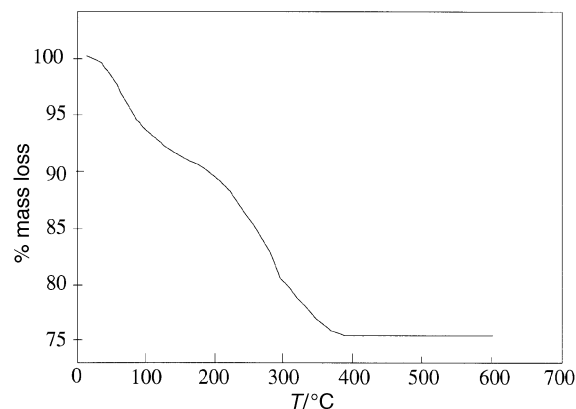


**Fig. 2** TGA curve for the  $[PPy]_{0.5}V_2O_5$  nanocomposite aerogel, heated at  $10^\circ C \text{ min}^{-1}$  in air

**Table 1** Comparison of physical and electrical properties for  $[PPy]_{2P}V_2O_5$  aerogels

composition	$[PPy]_{2P}V_2O_5$ $P$	$\rho/g \text{ cm}^{-3}$	$\sigma(25^\circ C)/S \text{ cm}^{-1}$	surface area/ $m^2 \text{ g}^{-1}$	oxidizing agent added
$V_2O_5$	0	0.10	$2 \times 10^{-4}$	150	no
$[PPy]_{0.6}V_2O_5$	0.3	0.19	$2 \times 10^{-4}$	184	no
$[PPy]_{0.6}V_2O_5$	0.3	—	—	257	yes
$[PPy]_{1.0}V_2O_5$	0.5	0.22	$2 \times 10^{-6}$	—	no
$[PPy]_{1.4}V_2O_5$	0.7	0.20	$4 \times 10^{-7}$	179	no
$[PPy]_{1.8}V_2O_5$	0.9	0.25	$2 \times 10^{-8}$	—	no
$[PPy]_{2.0}V_2O_5$	1.0	0.15	—	160	no
$[PPy]_{2.0}V_2O_5$	1.0	0.12	$2 \times 10^{-6}$	200	yes
microcomposite $[PPy]_{1.0}V_2O_5$	0.5	0.14	$3 \times 10^{-4}$	—	pre-polymerized
microcomposite $[PPy]_{2.0}V_2O_5$	1.0	0.18	$3 \times 10^{-4}$	140	pre-polymerized
microcomposite $[PPy]_{3.0}V_2O_5$	1.5	0.16	$3 \times 10^{-4}$	—	pre-polymerized
microcomposite $[PPy]_{6.0}V_2O_5$	2.0	0.19	$3 \times 10^{-4}$	80	pre-polymerized

We also undertook other synthetic strategies to prepare these nanocomposites, in an effort to examine the effect of inorganic–organic interaction. The second approach involved the addition of an aqueous dispersion of pre-polymerized polypyrrole to the vanadium alkoxide thus triggering hydrolysis of the alkoxide. Hydrolysis was sufficiently rapid (within 10 s) that the polymer particles were encapsulated in the  $V_2O_5$  gel network.

### Physical properties

BET analysis indicated that the surface areas of the nanocomposites prepared by simultaneous polymerisation are similar to that measured for pure  $V_2O_5$  ARGs. The  $[PPy]_{2P}V_2O_5$  samples exhibited surface areas of between 150 and  $250 \text{ m}^2 \text{ g}^{-1}$  (Table 1). The surface area of these pure  $V_2O_5$  ARGs is lower than that found previously ( $300\text{--}400 \text{ m}^2 \text{ g}^{-1}$ ) for samples synthesized under different precursor ratios.<sup>1</sup> Samples prepared by the dispersion method exhibited a slightly lower surface area of  $80\text{--}140 \text{ m}^2 \text{ g}^{-1}$  due to the presence of micrometre-sized PPy particles within the oxide matrix (*vide infra*).

Pure vanadium pentoxide ARGs are hydrated oxides of the composition  $V_2O_5 \cdot nH_2O$  with  $n=2.0\text{--}2.2$ . At approximately  $150^\circ C$ , the water layer between the fibers is no longer continuous and the conductivity of  $V_2O_5 \cdot nH_2O$  becomes essentially electronic. Fig. 2 shows a TGA curve for the  $[PPy]_{0.5}V_2O_5$  nanocomposite, in which two characteristic mass losses are observed. The initial step below  $125^\circ C$  is due to loosely bound water in the material. The remaining feature at  $250^\circ C$  is

attributed to a combined loss of water and PPy. This behavior is very similar to that reported for  $PPy/V_2O_5$  xerogels, for which PPy decomposition also occurs above  $250^\circ C$ .<sup>7</sup> Assuming that all of the PPy is combusted by  $400^\circ C$ , there are still *ca.* 1.2 moles of water remaining in the nanocomposites at  $180^\circ C$ . The composition of the as-prepared ARG nanocomposites can be calculated as  $PPy_{2P}V_2O_5 \cdot nH_2O$ , where  $P=0.15\text{--}1.0$  and  $n=2.4\text{--}3.1$ .

XRD studies showed that both  $V_2O_5$  and  $[PPy]V_2O_5$  ARGs exhibit a very low degree of crystallinity compared to the respective xerogel forms. The relatively amorphous structure resulted in a very broad, weak reflection corresponding to an interlayer spacing of *ca.*  $12.5 \text{ \AA}$ , similar to that reported previously for pure  $V_2O_5$  ARGs. Additional poorly resolved reflections in the region  $2\theta=6\text{--}9^\circ$  were observed, in the same region reported for PPy intercalated in  $V_2O_5$  xerogel galleries.<sup>7</sup> This results are suggestive of some intercalation of PPy in the ARG, albeit in a highly disorganized structure that is not amenable to X-ray study.

The poorly organized nature of the ARG nanocomposites was also very evident in the TEM micrographs. Whereas the fibers for the  $V_2O_5$  ARG displayed a long, ribbon-like structure similar to that previously reported for vanadate xerogels [Fig. 3(a)],<sup>1</sup> those of the polymer-ARG were much shorter in length, and were aggregated in a random fashion [Fig. 3(b)]. This morphology is substantially different than the ARG nanocomposites prepared using the dispersion method, which consisted of PPy particles encapsulated in the fibrous  $V_2O_5$

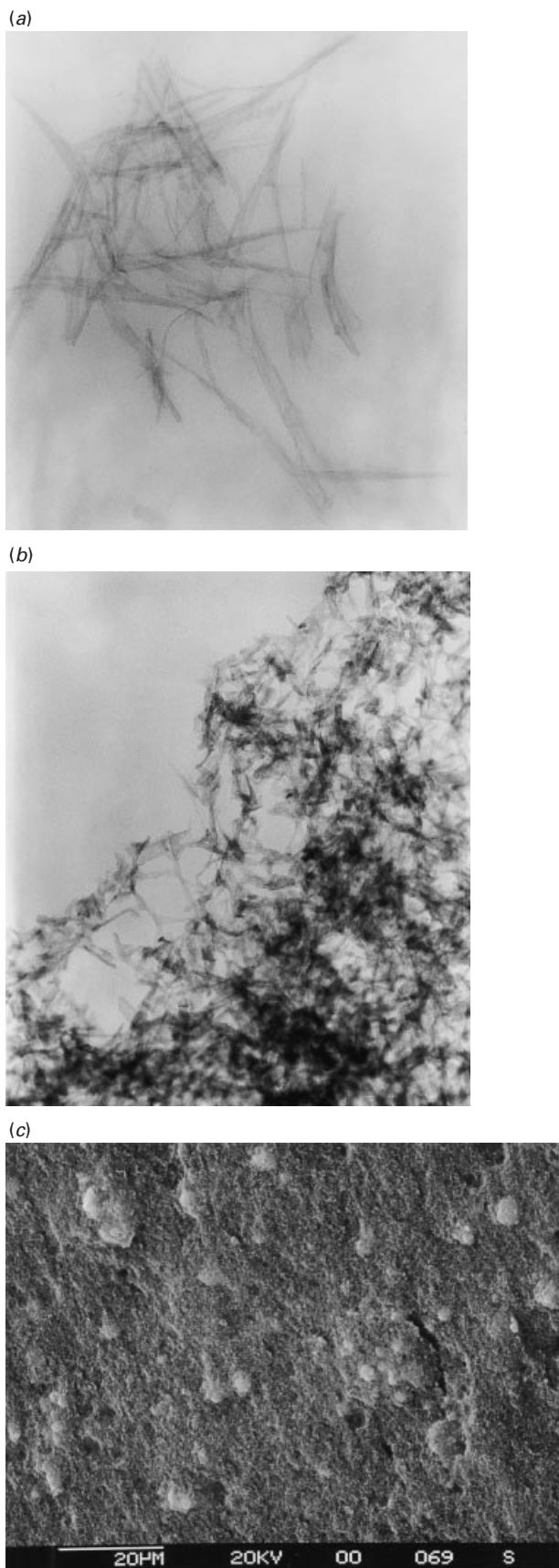


**Fig. 3** TEM micrographs (135K) of (a)  $V_2O_5$  aerogel; and (b)  $[PPy]_{0.5}V_2O_5$  nanocomposite aerogel prepared by simultaneous polymerisation, showing interrupted chain growth; (c) SEM micrograph of the  $[PPy]_{1.0}V_2O_5$  microcomposite prepared by the dispersion method

network, as shown by SEM [Fig. 3(c)]. Thus, the simultaneous copolymerisation method produces a nanocomposite that is characterized by almost molecular level mixing which appears to inhibit growth of the inorganic network. Conversely, the dispersion method produces what might be classified as a microcomposite.

#### FTIR analysis

The FTIR spectrum of the ARG nanocomposite between 2000 and  $400\text{ cm}^{-1}$  (not shown) displays strong bands in the  $1600\text{--}900\text{ cm}^{-1}$  region that are diagnostic of PPy, and their position and intensities show that the conductive form of the polymer is produced. The chain length and conductivity of the PPy can be estimated from the ratio of the A'/B' bands at  $1580$  and  $1460\text{ cm}^{-1}$  respectively. Studies of bulk PPy show a linear relationship between this ratio and the log of the conductivity of the polymer.<sup>15</sup> Using this data, together with the A'/B' value in the nanocomposite, ( $\cong 5.0$ ), interpolation indicates that the PPy component appears to be relatively conductive ( $1\text{ S cm}^{-1}$ ). The bands also exhibit slight shifts from those of bulk, p-doped PPy, suggesting that a substantial interaction with the  $V_2O_5$  framework occurs. More insight on the nature of this interaction is provided by examining the changes occurring in the vibrational modes of the inorganic lattice which dominate the spectrum.

Owing to the presence of V—O—V units, two vibrational modes, the symmetric stretch ( $\nu_{\text{sym}}$ ) and the asymmetric stretch ( $\nu_{\text{as}}$ ) are expected to occur in the vibrational spectrum in the range  $400\text{--}800\text{ cm}^{-1}$ .<sup>16</sup>  $^{18}\text{O}$  isotope shifts of samples prepared using  $^{18}\text{O}$ -labeled water were used to identify these modes. The band at  $542\text{ cm}^{-1}$  in the natural abundance sample (figure not shown) downshifts to  $521\text{ cm}^{-1}$  in the  $^{18}\text{O}$ -labeled samples. As the symmetric stretch of the M—O—M containing structures usually occurs in this region, this mode is assigned as  $\nu_{\text{sym}}$ . A low intensity peak at  $772\text{ cm}^{-1}$  is also found to shift upon  $^{18}\text{O}$  substitution and is tentatively assigned as  $\nu_{\text{as}}$ .

The assignment of these modes was used to characterize the structural changes associated with PPy incorporation. We found that both modes shift to higher wavenumber with increasing PPy content, with a direct correlation of upshift to PPy content (Table 1). The  $\nu_{\text{sym}}$  mode at  $542\text{ cm}^{-1}$  in the pristine  $V_2O_5$  sol-gel is increased to  $580\text{ cm}^{-1}$  in samples of  $PPy_{1.0}V_2O_5$  (Fig. 4). The data suggests a highly interacting

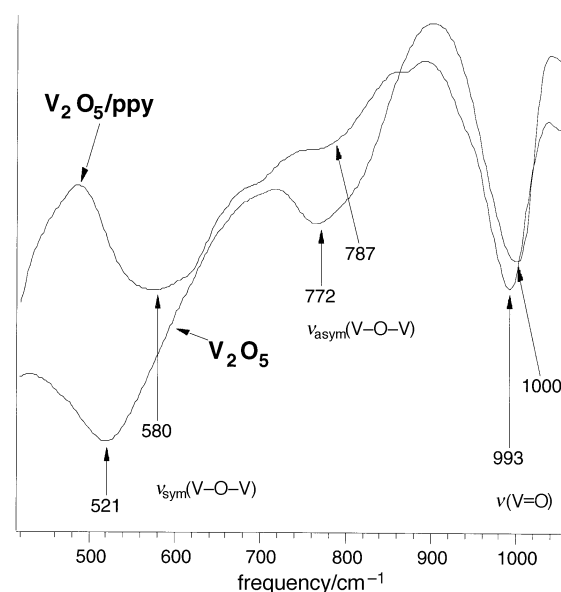


**Fig. 4** FTIR spectra comparing  $V_2O_5$  ( $^{18}\text{O}$ -labelled) and  $V_2O_5/PPy$  composite aerogels showing effects of PPy incorporation on  $\nu_{\text{sym}}(\text{V—O—V})$ ,  $\nu_{\text{as}}(\text{V—O—V})$  and  $\nu(\text{V=O})$

$V_2O_5$ -PPy host-guest system in which the coordination environment at the metal centers is affected by interaction with the organic component. Prior studies on  $V_2O_5$  reported by Savariault *et al.* with pyridine as an intercalant resulted in lowered frequencies of the  $V_2O_5$  modes in the 500–800  $cm^{-1}$  region.<sup>17</sup> The downshifts were ascribed to coordination of pyridine to vanadium ions which leads to weakening of the V–O–V bonds. Similar downshifts have also been observed with anilinium ion as a dopant.<sup>18</sup> Our data shows that intercalation of PPy induces a different mode of interaction with the  $V_2O_5$  matrix leading to a different structural perturbation of the matrix.

In contrast, the vanadyl stretch ( $\nu_{V=O}$ ) which occurs at 1000  $cm^{-1}$  in the  $V_2O_5$  ARG, shifts to 993  $cm^{-1}$  on incorporation of the polymer, implying either increased  $V^{4+}$  content in the lattice or a weakening of the V=O bond. Similar downshifts have been previously observed with pyridine and anilinium ions as intercalates in  $V_2O_5$ , and our results are in general agreement with vibrational data obtained with other N-containing species as intercalation guests (Table 2). In these cases the shifts are a result of reduced V–O–V bond length caused by weak binding of the nitrogen atom of the pyrrole ring to the sixth apical coordination site on the square-pyramidal V site.

For the PPy/ $V_2O_5$  nanocomposites, the major factor in the shift of the V=O band, however, is the contribution of H-bonding interactions. In order to determine the nature of the H-bonding interaction between the PPy polymer and the inorganic matrix, spectra were obtained on samples prepared in  $D_2O$ . FTIR spectra of pure  $V_2O_5$  materials show an absence of isotope shifts for the  $\nu(V=O)$  mode at 1000  $cm^{-1}$ , indicating a lack of hydrogen bonding interactions. This mode in [PPy]<sub>1.0</sub> $V_2O_5$  ARGs, however, shows sensitivity to deuterium substitution. The V=O mode at 993  $cm^{-1}$  downshifts to 987  $cm^{-1}$  in the  $D_2O$ -labeled samples (Fig. 5). The development of H-bonding interactions between the  $V_2O_5$  matrix and the polymer appears to be a principal factor for decreased V=O bond strength in the nanocomposite materials. Collectively, our results therefore suggest a presence of V=O...H type units in the nanocomposite materials. Significantly, both the shifts in the V–O–V bands, and the V=O bands were not observed in the microcomposite materials prepared by the dispersion method.

**Table 2** Effects of PPy intercalation upon  $\nu_{sym}(V-O-V)$

sample	$\nu_{sym}(V-O-V)/cm^{-1}$
$V_2O_5$	542
[PPy] <sub>0.4</sub> $V_2O_5$	565
[PPy] <sub>0.5</sub> $V_2O_5$	574
[PPy] <sub>1.0</sub> $V_2O_5$	580

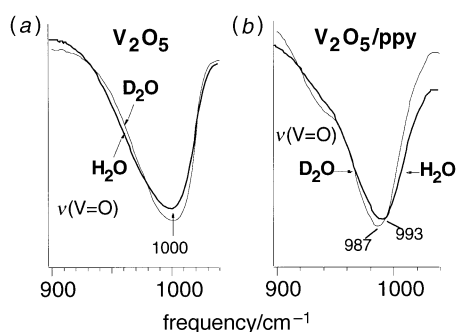


**Fig. 5** FTIR spectra of the V=O bond showing the effects of  $D_2O$  labelling: (a)  $V_2O_5$  aerogel; (b)  $V_2O_5$ /PPy composite aerogel

## Electrical properties

The nanocomposite samples were heat treated at 180°C prior to complex impedance measurements. TGA analysis showed that the nanocomposites lose 10% of their mass by this temperature, corresponding to a composition of [PPy]<sub>2P</sub> $V_2O_5 \cdot 1.2H_2O$ . The dispersion observed in the complex impedance plane indicates that there is an ionic contribution to the conductivity for samples with pyrrole ratios greater than  $P=0.7$ . At lower pyrrole contents, and in pure  $V_2O_5$ , only electronic conduction is observed. Moreover, the PPy/ $V_2O_5$  microcomposites prepared by the dispersion method also exhibited only electronic conduction.

Fig. 6 shows the results of the complex impedance analysis for both the nanocomposites and microcomposites. For the [PPy]<sub>2P</sub> $V_2O_5$  nanocomposites [Fig. 6(a)], the conductivity decreases with increasing PPy content. At 25°C, the conductivity decreases by a factor of  $10^4$  as  $P$  increases from 0 to 0.9 (Table 1). The activation energy changes only slightly from that of pure  $V_2O_5$  (0.23 to 0.32 eV). In contrast to this behavior, the microcomposites exhibit no change in conductivity from that of pure  $V_2O_5$  despite the fact they contain as much as 75 mol% PPy [Fig. 6(b)].

## Electrochemical lithium insertion in nanocomposite aerogels

**$V_2O_5$  aerogel.** In order to understand the effect of the PPy incorporation into the ARG,  $V_2O_5$ -ARG was first studied as an electrode material in a Li battery as a function of discharge depth, and cycling rate. The first discharge cycle is shown in Fig. 7(a) down to 1.8 V. Two Li potential sites are evident at 2.9 and 2.5 V *vs.* Li. Both sites are normally present in the

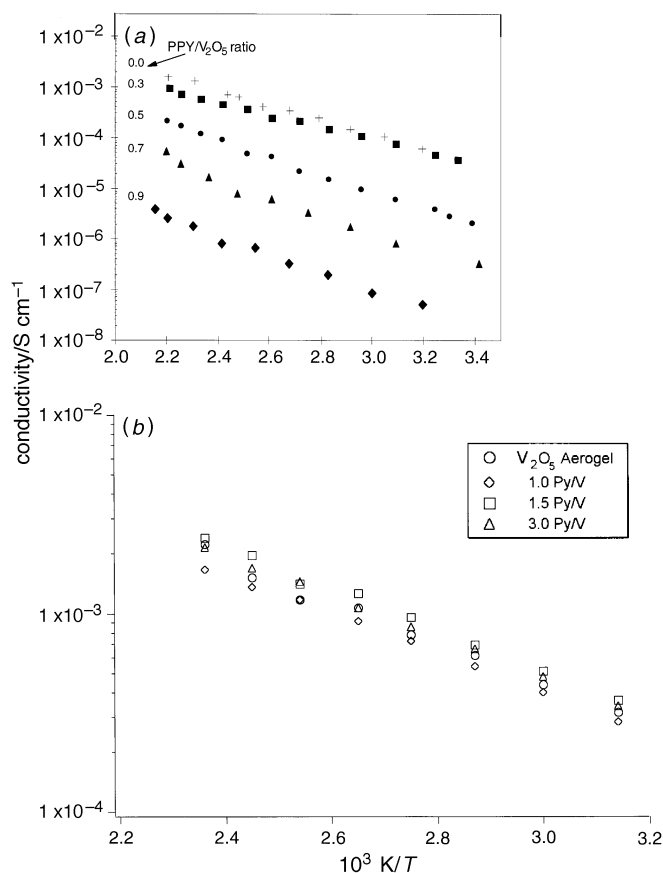


**Fig. 6** (a) Conductivity-temperature plot of [PPy]<sub>2P</sub> $V_2O_5$  aerogels where  $P=0-1$ . The + data points are for pure  $V_2O_5$  ( $P=0$ ); (b) conductivity-temperature plot of PPy/ $V_2O_5$  aerogels prepared by the dispersion method.

$V_2O_5$  xerogel. The corresponding mirror image of these redox peaks is observed in charge.

The second and third cycles were then recorded on decreasing the discharge cut-off voltage to 1.2 V *vs.* Li. An additional reduction process appears at 1.5 V, which modifies the subsequent charge process. By contrast to the first oxidation sweep, three defined oxidation peaks are now observed during the following charge (1.65, 2.15 and 2.65 V). This transformation continues in the following cycle in this 1.2–3.8 V window. On discharge, small shifts occur in the position of the reduction peaks. In charge, however, the lower potential Li site disappears, and a well defined site further develops at 2.15 V. Greater Li occupancy is also observed at higher voltage, marked by the presence of a large shoulder on the charge curve. Hence, we have found that these electrochemical processes are very sensitive to the reduction depth. The redox processes that we observe during the intercalation–deintercalation of Li are different from those reported by Smyrl *et al.* They do not observe the 2.5 V Li site either in discharge or in charge, as they did not cycle below 1.8 V.<sup>3b,c</sup>

Kinetic factors also play a role in the site occupancies. We have used cyclic voltammetry to examine the effect of rate on the relative site occupancies. For average to high cycling rates [10 mV (0.2 h)<sup>-1</sup> to 10 mV (0.02 h)<sup>-1</sup>] the ratio of the occu-

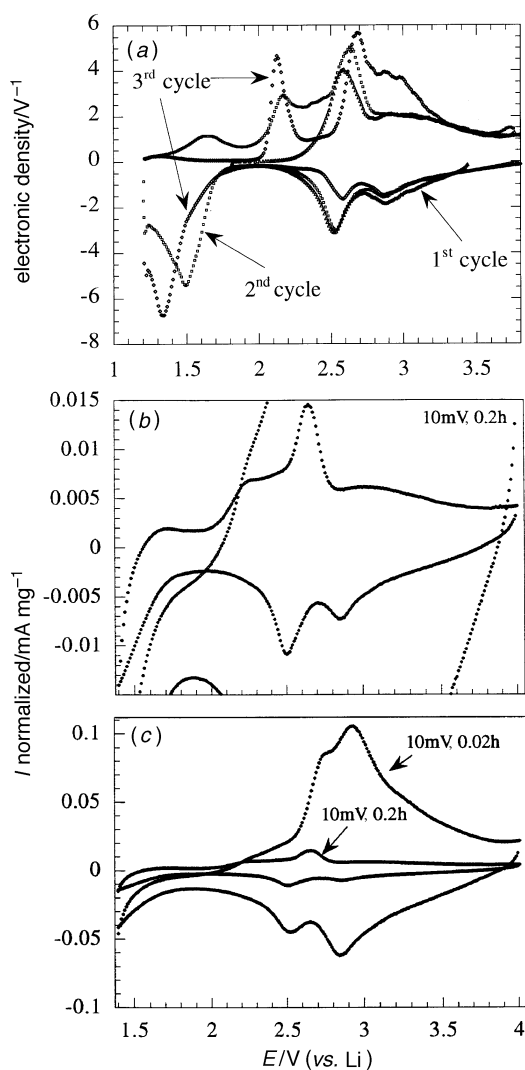


**Fig. 7** (a) Modification of the electronic density *vs.* voltage curves as a function of the discharge cut-off (1.8 and 1.2 V) for  $V_2O_5$ -ARG at  $10 \mu A cm^{-2}$ ; cycles are indicated on the plot; cyclic voltammograms of  $V_2O_5$ -ARG corresponding to a 10 mV/0.2 h voltage step, (b) and a 10 mV/0.02 h voltage step, (c) in the voltage window between 1.4 and 4.0 V.

pancies of the 2.5 and 2.9 V Li site in discharge is reversed [Fig. 7(b)]; nevertheless, the 2.5 V site is still present. The anodic peak at 2.15 V is particularly sensitive to the cycling rate, as it is not observed at the higher rate.

At the same cycling rate, the  $V_2O_5$ -ARG performs better than the xerogel, as previously reported. Even though the theoretical capacity is lower for the aerogel than for the xerogel (owing to a greater contribution of  $V^{4+}$ ), the experimental Li capacity is a factor 1.7 times greater (1.105 and 1.80 F mol<sup>-1</sup> for  $V_2O_5$ -XRG and ARG, respectively). This outlines the importance of the kinetic factors, and shows that there is excellent accessibility of Li sites in this high surface area material. Furthermore, the  $V_2O_5$ -ARG displays good stability in the 1.2–4.0 V window, giving a specific capacity of 400 mA h g<sup>-1</sup> under these conditions.

**Effect of PPy content on the electrochemical response.** The dependence of the voltage *vs.* first discharge capacity as a function of the polymer content is shown on Fig. 8. The effect of the PPy on the electrochemical response is to clearly decrease the Li capacity, in accordance with the electrical measurements which showed decreased conductivity as a function of polymer content. In the electrochemical sense, this can be explained by a lowering of the oxidation potential of the vanadium oxide component (*via* increased formation of  $V^{4+}$ ) as a result of *in situ* reaction with the pyrrole monomer (*vide infra*).

The modification of the Li sites on polymer incorporation is illustrated in Fig. 9. The nanocomposites display two distinct processes in discharge, shifted to some degree from their respective positions in  $V_2O_5$ . [PPy]<sub>0.3</sub> $V_2O_5$  is different from the other compositions, in that Li occupies the 2.5 and 2.9 V

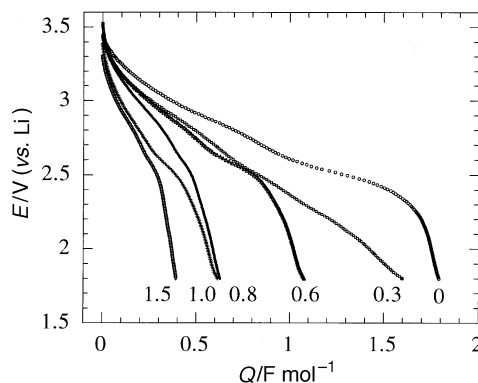


**Fig. 8** Evolution of the first discharge curves as function of the polymer content ( $2P$ ), in  $[PPy]_yV_2O_5$  at  $10 \mu A cm^{-2}$

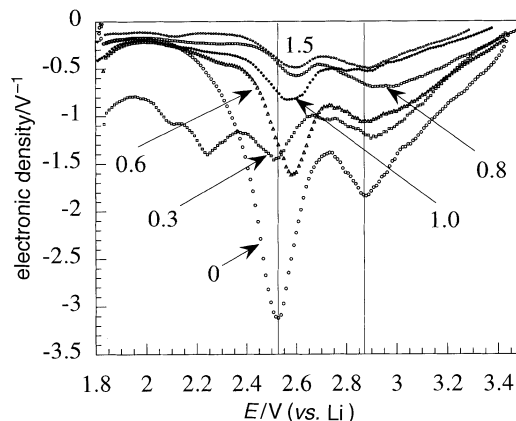


**Fig. 9** Evolution of the electronic density *vs.* voltage curves as a function of the polymer content in the nanocomposites. The curves were obtained by numerical differentiation of the plots shown in Fig. 8.

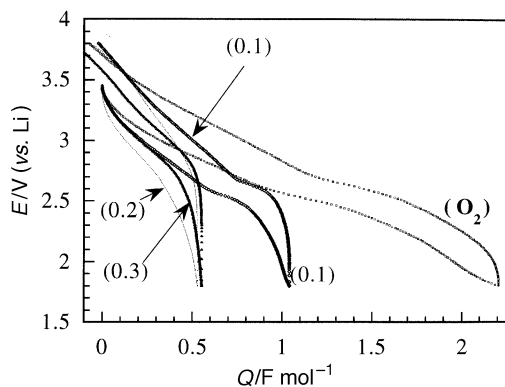


**Fig. 10** Effect of the oxidative treatment on  $[\text{PPy}]_{0.3}\text{V}_2\text{O}_5$ ; discharge-charge curves are shown for materials prepared using an *in situ* oxidative treatment with molar ratios  $(\text{NH}_4)_2\text{S}_2\text{O}_8/\text{V}_2\text{O}_5$  of 0.1, 0.2 and 0.3. The fourth curve shows  $[\text{PPy}]_{0.3}\text{V}_2\text{O}_5$  after  $\text{O}_2$  treatment for comparison. A cycling rate corresponding to the intercalation of 1.0 Li in 20 h ( $C/20$ ) was used.

Li sites as in  $\text{V}_2\text{O}_5$ , in addition to two new sites at 2.1 and 2.25 V. Li insertion in the nanocomposites gives rise to broader reduction peaks, and hence the sites are less well ordered than in  $\text{V}_2\text{O}_5$ . The same factor has been observed for xerogel-derived  $[\text{PPy}]\text{V}_2\text{O}_5$ , in which incorporation of the polymer results in a wider distribution of the Li site potential.<sup>8b,c</sup>

**Effect of an oxidation treatment.** We attempted to offset the lower capacity of the nanocomposite ARGs by reoxidizing the material. Two different oxidation treatments were carried out; *in situ* and post-oxidation. The effect of these treatments on the  $[\text{PPy}]_{0.3}\text{V}_2\text{O}_5$  electrochemical response is displayed in Fig. 10. The *in situ* method in which the oxidizing agent (persulfate) is involved during the formation of the nanocomposite, had a negative effect on the electrochemical response. The *in situ* oxidized materials give rise to a lowered Li capacity of  $<1 \text{ F mol}^{-1}$ , suggesting that though the vanadium is in a higher oxidation state in this case, the Li ions do not have access to the redox centers.

On the other hand, after post-oxidative treatment under oxygen, the capacity of the nanocomposite is significantly improved (curve 4, Fig. 10), yielding a fully reversible capacity of  $2.2 \text{ F mol}^{-1}$ . Step potential electrochemical spectroscopy (SPES) experiments show that a better occupancy of the 2.5 V Li site is mostly responsible for the enhanced capacity of the  $\text{O}_2$  treated material. Moreover, this material is capable of rapid Li ion diffusion at high cycling rates. These results will be described more fully in a subsequent publication.

## Discussion

### Nature of the $\text{V}_2\text{O}_5$ -PPy interaction

The TEM, conductivity and FTIR results collectively point to an intimate and strong interplay of the inorganic and organic components in the nanocomposite material, as opposed to the microcomposite material. There are two types of vibrational modes whose shifts indicate the nature of the interaction. The shifts of the  $\nu(\text{V}=\text{O})$  modes indicate that increased H-bonding effects are observed in the nanocomposite material. The H-bonding upon PPy incorporation can be ascribed to interaction with the organic moiety. The NH functional group in the PPy is an excellent candidate for an H-bonding interaction. Acid-base type reactions between a basic dopant and the  $\text{V}_2\text{O}_5$  framework have been previously proposed as the dominant mode of interaction.<sup>19</sup> The strong H-bonding interactions between the NH group of PPy and the  $\text{V}=\text{O}$  moiety represent a limiting example of such interactions. We propose a tentative model of the interactions that may be operative in the nanocomposite materials in Fig. 11.

The second type of vibrational mode that is affected by the interaction is the  $\text{V}-\text{O}-\text{V}$  stretch. Prior studies on intercalation of N-containing species indicate that the  $\text{V}-\text{O}-\text{V}$  modes are downshifted upon introduction of the guest species. The observed upshifts of both the vibrational modes,  $\nu_{\text{sym}}(\text{V}-\text{O}-\text{V})$  and  $\nu_{\text{as}}(\text{V}-\text{O}-\text{V})$ , on PPy incorporation is consistent with increased bond strengths of the bridging  $\text{V}-\text{O}-\text{V}$  groups in the composite. This cannot be attributed to increased  $\text{V}^{4+}$  content in the materials as a result of reaction with the pyrrole monomer. Although the electrochemistry results (*vide infra*) confirm the increasing formation of  $\text{V}^{4+}$  with increasing polymer content, it is evident that another effect dominates the shifts in the IR bands. One tentative mechanism that may account for the observed increase in  $\text{V}-\text{O}-\text{V}$  bonding interaction is based on the change in coordination geometry at the metal center. The vanadium ions in  $\text{V}_2\text{O}_5$  adopt a square pyramidal coordination with the V atoms occupying a position slightly above the basal plane.<sup>20</sup> The distorted geometry is facilitated by the strong  $\text{V}=\text{O}$  interaction. A decrease in  $\text{V}=\text{O}$  interaction in the nanocomposite material is likely to alter the coordination geometry. A change in position of the V ion, caused by decreased axial interaction, such that it occupies a position in the  $\text{VO}_4$  plane will result in increased in-plane bonding interactions. The  $\text{V}-\text{O}-\text{V}$  groups in the  $\text{V}_2\text{O}_5$ -based materials lie in the plane and the strong H-bonding induced elongation of  $\text{V}=\text{O}$  bond is likely to induce structural distortions at the metal center that can account for the observed strengthening of the  $\text{V}-\text{O}-\text{V}$  bonds.

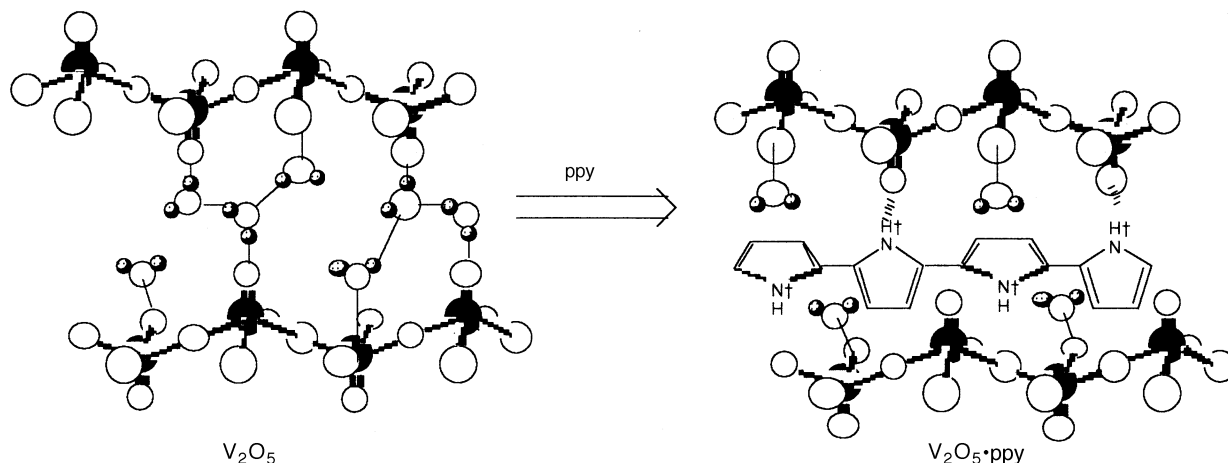


**Fig. 11** Illustration showing proposed interaction of the PPy with the  $\text{V}_2\text{O}_5$  framework

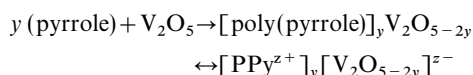
## Influence of the interaction

The experimental results indicate that the interaction influences at least three different physical properties; the microstructure, the electrical conductivity and the electrochemical response.

We chose a simultaneous polymerisation method for the formation of the nanocomposites, as prior work has shown that it leads to optimum mixing at the molecular level, and hence a homogeneous matrix. In this system, polymerisation to form the PPy network is effectively caused by a redox reaction with the inorganic component, leading to the formation of  $V^{4+}$  which in turn catalyzes the rate of the condensation of the  $V_2O_5$  network. The latter effect is well known for the corresponding  $V_2O_5$  xerogels.<sup>2,21</sup> It is demonstrated here by the considerably shorter gelation time for the system. Thus we have a 'double' polymerisation process that results in a homogeneous composite as desired, but one in which the rapid polymerisation rate of the inorganic polymer leads to interrupted growth of the characteristic ribbon morphology of  $V_2O_5$ , as shown in the TEM photomicrographs.

The microstructure of the organic-inorganic nanocomposite has a profound effect on the electrical conductivity. In the case of simultaneous polymerisation, the truncation of this fibrous structure by interaction with the occluded PPy disrupts charge transport within the continuous  $V_2O_5$  phase. We see a direct correlation of lower conductivity with increased PPy content, and shift of the  $\nu_{\text{sym}} V-O-V$  band. Conversely, the dispersion method leads to isolated PPy particles encapsulated in the continuous  $V_2O_5$  phase. In this case, the addition of PPy has no effect on the gelation rate of the  $V_2O_5$ , enabling the characteristic  $V_2O_5$  ribbon structure to develop. Thus, the observed conductivities are independent of PPy content and comparable to that of the pristine  $V_2O_5$  ARG. The expected conductivity increase upon addition of the conductive polymer was not observed because the particles were effectively isolated and did not form a continuous phase within the matrix.

A third influence of the PPy- $V_2O_5$  interaction is that on the electrochemical Li insertion properties. The formation of PPy leads to the creation of  $V^{4+}$  centers, and therefore decreases the Li capacity. In principle, two electrons are lost from the  $V_2O_5$  in the coupling of each monomer unit in the polymerisation step:



Although the second oxidation step (doping) represents a reversible redox process from a thermodynamic point of view, the first step does not. The linear variation of the first discharge capacity with PPy content (Fig. 8) reflects this. Note that the observed capacity decreases are what one would predict from consideration of the polymer ratio and the two electron reduction process above, starting from a partially reduced  $V_2O_5$  lattice (ca. 10%  $V^{4+}$ ), in combination with some reoxidation of the V centers by exposure to air.<sup>6b</sup>

As these materials possess a mixed valence  $V^{5+}/V^{4+}$  state counterbalanced by the presence of mobile species (protons) and oxidizable polymer, it was of interest to investigate the effect of subjecting the electrode to an initial oxidation (charge process). During this process, oxidation of redox centers from  $V^{4+}$  to  $V^{5+}$  can occur, along with possible additional doping of the polymer involving further oxidation. In either case, electrochemical oxidation would be accompanied by expulsion of  $H^+$  or insertion of  $ClO_4^-$  anions. No well defined oxidation peak was observed for an initial charge up to 3.8 V, although a gain in total reversible capacity was observed. For nanocomposites with a small PPy content  $0 < P < 0.6$ , the capacity increase during the charge process is almost what one would expect from reoxidation of the reduced components. For example, the capacity of  $[PPy]_{0.3}V_2O_5$  increases from 1.6 to 1.85  $F \text{ mol}^{-1}$  during charge.

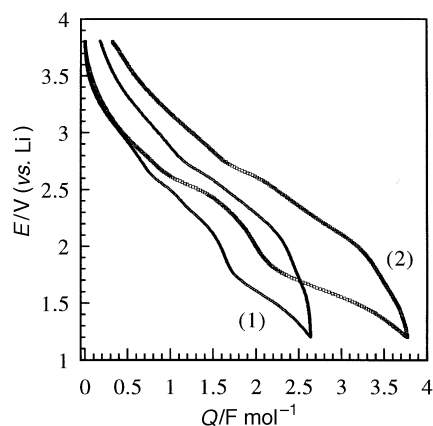


Fig. 12 Voltage vs. composition curves for the post-oxidation of aerogel electrodes in the 3.8–1.2 V window, at a constant current of  $10 \mu A \text{ cm}^{-2}$ . (1)  $V_2O_5$  aerogel; (2) the post-oxidized nanocomposite aerogel  $O_2-[PPy]_{0.3}V_2O_5$ .

At higher PPy ratios (where  $P > 0.6$ ), the gain in capacity is less than expected, and dependent on whether the oxidation precedes or follows the discharge process. This behavior has been previously observed in the electrochemical response of polymer/ $V_2O_5$  xerogels (polymer = polythiophene and polypyrrole) and was attributed to restricted access of  $Li^+$  owing to blockage by excessive surface polymer.<sup>8b,c</sup>

Chemical oxidation can be used to even greater benefit, to regain the lost capacity in these materials, similar to that observed previously for polymer/ $V_2O_5$  xerogels.<sup>8a,b</sup> In particular, the post-oxidative treatment drastically improves the electrochemical response *via* direct effect on the redox centers, and gives rise to increased capacity for  $O_2-[PPy]_{0.3}V_2O_5$  (2.2  $F \text{ mol}^{-1}$  to a discharge voltage of 1.8 V). At a wider voltage window of 3.8–1.2 V (Fig. 12), the capacity of the pristine  $V_2O_5$  ARG is 2.7  $F \text{ mol}^{-1}$ , and is increased to 3.8  $F \text{ mol}^{-1}$  for the  $O_2$ -treated  $[PPy]_{0.3}V_2O_5$  nanocomposite.

A more detailed comparison of the electrochemical behaviour of this system with that of the 'microcomposite' PPy- $V_2O_5$  will be reported in a subsequent paper.<sup>22</sup>

## Conclusions

Polypyrrole/vanadium pentoxide aerogel materials were synthesized by two different sol-gel routes with the simultaneous polymerisation method being investigated in greater detail. The resulting organic-inorganic materials are typical of ARGs in that they possess low density ( $0.1\text{--}0.2 \text{ g cm}^{-3}$ ) and high surface area ( $150\text{--}250 \text{ m}^2 \text{ g}^{-1}$ ). The materials are characterized by strong interactions between the organic and inorganic components which influence the electrical and electrochemical properties of the nanocomposite. This interaction is evident by shifts in the  $V=O$  and  $V-O-V$  modes and is attributed to strong H-bonding interactions and alteration of the coordination geometry, respectively. This interaction and changes in the aerogel microstructure lead to progressively lower electrical conductivity upon addition of PPy to the nanocomposite. Since the formation of PPy leads to creation of  $V^{4+}$  centres, lithium capacity decreases with PPy content. This lost capacity is regained by oxidation treatments, however. The electrochemical results demonstrate the ability of PPy/ $V_2O_5$  aerogel nanocomposites to exhibit a substantial improvement in lithium capacity as compared to the pristine oxide.

The financial support of this research by the Office of Naval Research (B.D.) and the Natural Sciences and Engineering Council of Canada (L.F.N.) is gratefully acknowledged.



## References

- 1 F. Chaput, B. Dunn, P. Fuqua and K. Salloux, *J. Non-Cryst. Solids*, 1995, **188**, 11.
- 2 J. Livage, *Chem. Mater.*, 1991, **3**, 578.
- 3 (a) B. Katz, W. Liu, K. Salloux, F. Chaput, B. Dunn and G. C. Farrington, *Mater. Res. Soc. Symp. Proc.*, 1995, **369**, 211; (b) D. B. Le, S. Passerini, A. L. Tipton, B. B. Owens and W. H. Smyrl, *J. Electrochem. Soc.*, 1995, **142**, L102; (c) D. B. Le, S. Passerini, J. Guo, J. Ressler, B. B. Owens and W. H. Smyrl, *J. Electrochem. Soc.*, 1996, **143**, 2101.
- 4 B. Scrosati, in *Solid State Electrochemistry*, ed. P. G. Bruce, Cambridge University Press, Inc., Cambridge, 1995, p. 229.
- 5 S. Panero, E. Spila and B. Scrosati, *J. Electrochem. Soc.*, 1996, **143**, L29; K. Naoi, M. Lien and W. H. Smyrl, *J. Electrochem. Soc.*, 1991, **138**, 440.
- 6 (a) M. Kanatzidis, C-G Wu, H. O. Marcy and C. R. Kannewurf, *J. Am. Chem. Soc.*, 1989, **111**, 4139; (b) C-G. Wu, D. C. DeGroot, H. O. Marcy, J. L. Schindler, C. R. Kannewurf, Y. J.-Liu, W. Hirpo and M. Kanatzidis, *Chem. Mater.*, 1996, **8**, 1992.
- 7 C-G. Wu, M. Kanatzidis, H. O. Marcy and C. R. Kannewurf, *Polym. Mater. Sci. Eng.*, 1989, **61**, 969.
- 8 (a) F. Leroux, B. E. Koene and L. F. Nazar, *J. Electrochem. Soc.*, 1996, **143**, L181; (b) F. Leroux, G. R. Goward and L. F. Nazar, *J. Electrochem. Soc.*, 1997, **144**, 3886; (c) G. R. Goward, F. Leroux and L. F. Nazar, *Electrochimica Acta*, in press.
- 9 B. E. Koene and L. F. Nazar, *Solid State Ionics*, 1996, **89**, 147.
- 10 T. A. Kerr, H. Wu and L. F. Nazar, *Chem. Mater.*, 1996, **8**, 2005; L. F. Nazar, H. Wu and W. P. Power, *J. Mater. Chem.*, 1995, **5**, 1985.
- 11 B. C. Dave, B. Dunn, F. Leroux, L. F. Nazar and H. P. Wong, *Mater. Res. Soc. Symp. Proc., Better Ceramics Through Chemistry VII*, 1996, **435**, 611.
- 12 S. Maeda and S. P. Armes, *J. Colloid Interface Sci.*, 1993, **159**, 257; S. Maeda and S. P. Armes, *J. Mater. Chem.*, 1994, **4**, 935; S. Kuwabata, A. Kishimoto, T. Tanaka and H. Yoneyama, *J. Electrochem. Soc.*, 1994, **141**, 10; A. H. Gemeay, H. Nishiyama, S. Kuwabata and H. Yoneyama, *J. Electrochem. Soc.*, 1995, **142**, 4190.
- 13 W. A. Wampler, K. Rajeshwar, R. G. Pethe, R. C. Hyer and S. C. Sharma, *J. Mater. Res.*, 1995, **10**, 1811.
- 14 R. E. Myers, *J. Electron. Mater.*, 1986, **15**, 61.
- 15 J. Lei, Z. Cai and C. R. Martin, *Synth. Met.*, 1992, **46**, 53; J. Lei, Z. Cai and C. R. Martin, *ibid.*, 1992, **48**, 301.
- 16 M. R. Bond, R. S. Czernuszewicz, B. C. Dave, Q. Yan, M. Mohan, R. Verastegue and C. Carrano, *Inorg. Chem.*, 1995, **34**, 5857.
- 17 J.-M. Savariault, D. Lafargue, J.-L. Parise and J. Galy, *J. Solid State Chem.* 1992, **97**, 169.
- 18 Y.-J. Liu, D. C. DeGroot, J. L. Schindler, C. R. Kannewurf and M. G. Kanatzidis, *J. Chem. Soc., Chem. Commun.*, 1993, 593.
- 19 E. Ruiz-Hitzky and B. Casal, *J. Chem. Soc., Faraday Trans.*, 1986, **82**, 1597.
- 20 T. Yao, Y. Oka and N. Yamamoto, *Mater. Res. Bull.*, 1992, **27**, 669; P. Aldebert, N. Baffier, N. Gharbi and J. Livage, *Mater. Res. Bull.*, 1981, **16**, 669.
- 21 J. Lemerle, L. Nejem and J. Lefebvre, *J. Chem. Res.*, 1978, 5301.
- 22 B. Dunn, J. Herreld, F. Leroux, L. F. Nazar and K. Salloux, manuscript in preparation.

Paper 7/06614G; Received 10th September, 1997